Published in final edited form as:
Dev Biol. 2007 April 15; 304(2): 508–524.

Gene targeting reveals the role of Oc90 as the essential organizer of the otoconial organic matrix

Xing Zhao[1,*], **Hua Yang**[1,*], **Ebenezer N Yamoah**[2], and **Yunxia Wang Lundberg**[1,#]

1*Genetics Department, Boys Town National Research Hospital, Omaha, NE68131, USA*

2*Center for Neuroscience, Communication Science Program, University of California at Davis, Davis, CA 95616*

Abstract

A critical part of the functional development of our peripheral balance system is the embryonic formation of otoconia, composite crystals that overlie and provide optimal stimulus input to the sensory epithelium of the gravity receptor in the inner ear. To date neither the functions of otoconial proteins nor the processes of crystal formation are clearly defined. Using gene targeting and protein analysis strategies, we demonstrate that the predominant mammalian otoconin, otoconin-90/95 (Oc90), is essential for formation of the organic matrix of otoconia by specifically recruiting other matrix components, which includes otolin, a novel mammalian otoconin that we identified to be in wildtype murine otoconia. We show that this matrix controls otoconia growth and morphology by embedding the crystallites during seeding and growth. During otoconia development, the organic matrix forms prior to $CaCO_3$ deposition and provides optimal calcification efficiency. Histological and ultrastructural examinations show normal inner ear epithelial morphology but reduced acellular matrices, including otoconial, cupular and tectorial membranes, in Oc90 null mice, likely due to an absence of Oc90 and a profound reduction of otolin. Our data demonstrate the critical roles of otoconins in otoconia seeding, growth and anchoring and suggest mechanistic similarities and differences between otoconia and bone calcification.

Keywords

Otoconia; calcification; otoconin-90; otolin; fetuin-A; cupula; otoconial membrane; tectorial membrane

Introduction

The inner ear houses three mechanoreceptor organs: the cochlea, which detects sound; the three semi-circular canals, which detect rotational acceleration; and the utricle and saccule, which sense linear acceleration and gravity. Under the stimuli of sound or motion, the specific sensory epithelia are displaced relative to distinct acellular matrices, causing the stereocilia of the sensory hair cells to deflect and subsequently leading to the opening of mechanotransduction channels and depolarization of the cell. Only the utricle and saccule have an extremely dense

[#]Corresponding author: Yunxia Wang Lundberg, Ph. D., Genetics Department, Boys Town National Research Hospital, Omaha, NE 68131, Ph : 1-402-498-6735, Fax : 1-402-498-6351, Email: lundbergy@boystown.org
[*]X. Z. and H. Y. contributed equally to the work.

matrix, the otoconial complex, which provides inertial mass to generate shearing forces essential for the macular mechanoreceptors to sense gravity and linear acceleration.

The correct formation of otoconia is important for our sense of gravitation and linear acceleration, which is critical for spatial orientation and balance. Otoconial crystals are partially embedded in an amorphous gelatinous layer above the innermost meshwork layer. Electrophysiological and behavioral studies show that the density of the crystals affect the amount of stimulus input to the sensory hair cells and that significantly altered crystal mass or location invariably leads to behavioral deficits (Anniko et al., 1988;Jones et al., 1999;Jones et al., 2004;Kozel et al., 1998;Simmler et al., 2000;Sollner et al., 2004;Trune and Lim, 1983). In the clinical conditions canalithiasis and cupulolithiasis, dislocated otoconia become associated with the posterior crista and modify its physical responses such that the patients suffer from dizziness known as benign paroxysmal positional vertigo, BPPV, the most common cause of vertigo (Salvinelli et al., 2004;Squires et al., 2004). BPPV is usually referred to as BPV, benign positional vertigo.

Otoconia from higher vertebrates have a predominantly organic core with a lower level of Ca^{2+} and a largely inorganic periphery with a higher level of Ca^{2+}. The periphery consists of crystallites outlined by the organic matrix (Lins et al., 2000;Steyger and Wiederhold, 1995). The organic components primarily consist of glycoproteins (collectively called otoconins) and proteoglycans [with glycosaminoglycans (GAGs) side chains and glycogen derivatives in the proteoglycans] (Endo et al., 1991;Ito et al., 1994;Pisam et al., 2002;Pote and Ross, 1991;Verpy et al., 1999;Wang et al., 1998), and the inorganic component is primarily $CaCO_3$ (Carlstrom D, 1963). Both otoconia and fish otolith have internal and external fibrous structures of varied organizations, albeit much finer in otoconia. Recent studies in fish show that these fibers are likely made up of the inner ear-specific collagen called otolin (aka otolin-1) (Davis et al., 1997;Murayama et al., 2002). The predominant crystal core protein in bony fish, otolith matrix protein (OMP), was found to recruit otolin (Murayama et al., 2005). In mammals, the mechanisms for the formation of the core are unknown. The principal core protein is otoconin-90 (Oc90, aka Oc95) in mammals and birds and Oc22 in amphibians. Oc22 and Oc90 have 25-34% of amino acid similarity to secretory phospholipase A2 (PLA2), both group II and I. Oc22 has one PLA2-like domain (PLA2L) whereas Oc90 has two. Oc90 is similar to zebrafish OMP in several aspects: both are glycosylated and rich in cysteine residues that may form multiple disulfide bridges to provide a rigid structure as a scaffold for $CaCO_3$ deposition; both bind bivalent cations and both are expressed in all of the squamous non-sensory epithelium of the developing otocyst (Murayama et al., 2004;Murayama et al., 2005). However, mechanisms of crystal formation in fish and mammals likely differ due to differences in endolymph compositions and mechanosensation. For example, fish otoliths grow continuously throughout adulthood; fish endolymph is subjected to ionic changes in the water because of the ionic exchange through the gill epithelium. In this study, we used gene-targeting and protein analysis strategies to examine the role of Oc90 in mammalian otoconia formation and to provide some mechanistic information for the calcification process.

Materials and Methods

Generation of an Oc90 targeting construct (Figure 1)

For homologous recombination, two recombination arms, 5'-ARM (a 4.8 kb fragment spanning the region from introns 2-4) and 3'- ARM (2.9 kb, spanning introns 13-14), were amplified by long-PCR from 129/Ola (E14 line) genomic DNA using a long-PCR kit (Roche Applied Science). They were then unidirectionally cloned into the pPNT vector (constructed by Drs. C. Paszty, and V. Tybulewicz) using *Kpn* I and *EcoR* I for the 5'-ARM and *Xho* I and *Not* I for the 3'-ARM. The restriction sites were built into the PCR primers. The construct was confirmed by restriction mapping using *Xba* I and by sequencing of insert boundaries. Since

the secretion signal peptide of Oc90 remains, any remaining residual product would be secreted, therefore the *lacZ* gene was not inserted. We designed this to minimize any potential confounding effects of *lacZ* expression. After homologous recombination, we deleted exons 5-13, the entire first PLA_2L domain and most of the putative functional region of the second PLA_2L domain. The deletion creates an out-of-frame mutant transcript with 186 bp due to a premature stop codon (or 201 bp if an alternative start codon is used). The mutant protein has 50 aa (amino acids) after the signal peptide (38 wt N-terminal aa +12 mutant aa) with an estimated theoretical mass of 6.6 kD.

Electroporation of 129/Ola ES cells was done at the University of Nebraska Medical Center Mouse Genome Engineering Core Facility. Two probes, 5' and 3' external to the recombination arms, were used in Southern blotting to screen for targeted ES cell clones. For Southern blotting, *AlwN* I was used to digest ES cell DNA for hybridization with the 5'-probe and *Sph* I for the 3'-probe. The identified ES clones were expanded and Southern blotting was performed a second time (Figure 1B) to ensure that the correct ID of the ES clone was being expanded. The confirmed targeted clone 1A6 was injected into C57BL/6J blastocysts at the above core facility.

Southern blotting

Genomic DNA was prepared using a Mouse Tail Kit (Puregene). Twenty micrograms of each sample was digested with an appropriate enzyme at 37°C overnight and electrophoresed on a 0.8% agarose gel. Samples in the gel were then transferred under vacuum for 2 hours to a nylon membrane (Roche Applied Science) and cross-linked by baking at 120°C for 30 minutes. Digoxygenin (DIG)-labeled probes for blotting were generated by PCR using a DIG-labeling kit from Roche Applied Science. Hybridization and detection reagents were also supplied by Roche and procedures were carried out according to the manufacturer's manual. The hybridized and washed membrane was exposed to a Kodak X-ray film for signal detection.

Mouse genotyping and histology

The Oc90 null allele was backcrossed into C57BL/6J (Jackson Laboratory). All animal procedures were approved by the Institutional Animal Care and Use Committee at the Boys Town National Research Hospital in accordance with federal guidelines. Mouse tail DNA was used for genotyping by multiplex PCR and Southern blotting. PCR genotyping primers are denoted by unfilled block arrows in Figure 1Aand were 5'-TCTAACATCCCATTGCCCAGAGGA-3', 5'-CCAGCCTGACCTGTTCCTTTGTT-3' and 5'-AATATCACGGGTAGCCAACGCTATGTC-3' (from *Neo* gene). The first and second primers amplify the wt (wildtype) allele; the second and third primers amplify the null allele. Genotypes of a subset of the initial offspring were also confirmed by Southern blotting (Figure 1D).

For timed-mating, embryos were staged by designating the morning when the vaginal plug was found as E0.5. To harvest embryos, pregnant dams were euthanized with compressed CO_2. Embryos were dissected out of the uterus, separated from extra-embryonic membranes before fixation. Depending on the stage, either whole embryos or inner ears were fixed in 4% paraformaldehyde and embedded in paraffin for sectioning. Some inner ears were decalcified or partially decalcified in 0.1 M EDTA (pH7.4) for 2 hours to overnight, depending on the age of the animals. For whole mount studies, inner ears were dissected from fixed and decapitated embryos. For some otoconia morphological observation (including X-ray powder diffraction), protein analysis (protein identification and Western blotting) and RT-PCR, fresh unfixed tissues were used.

For histological staining and immunohistochemistry with older mice, animals were perfused with 4% paraformaldehyde, inner ears dissected, some of them decalcified in 0.1 M EDTA (pH7.4), dehydrated, embedded in paraffin and sectioned at 6μm. To obtain semi-thin (500 nm) and ultra-thin (85 nm) sections, inner ear epithelial tissues were embedded in resin (see below).

For phalloidin staining, fixed inner ears or paraffin-embedded sections (6μm) were permeabilized with 0.1% Triton X-100 in phosphate buffered saline (PBS), washed 3 or more times with PBS, and stained with a 50μg/ml Alexa-488 conjugated phalloidin solution (Sigma) in PBS (containing 1% DMSO from the original stock solution) for 40 minutes at room temperature (RT). Unbound conjugated phalloidin was washed several times with PBS and tissues were viewed using a Zeiss LSM 510 confocal microscope.

For Alizarin red complexone (ARC) staining, fixed whole mount tissues or sections (6μm) were stained with 1:50 dilutions (in PBS) of 0.5% Alizarin red complexone (Sigma) in 0.2 M KOH for 2 hours or overnight at RT. After washing off excess staining reagents, tissues/sections were viewed using a Zeiss LSM 510 confocal microscope.

Fluorescent immunostaining

Tissue sections were blocked in blocking solution containing 5% goat serum and 0.2% Triton-X-100 at RT for 30 minutes. Primary antibodies were added at a dilution of 1:400 or 1:600, and incubated at 4°C overnight. After 3 washes in 1×PBS, an Alexa-488 or 568 (Molecular Probes) conjugated goat anti-rabbit secondary antibody was added at a dilution of 1:250 and incubated at RT for 2 hours in the dark. Oc90 null tissues and/or pre-immune sera at the same dilutions as the primary antibodies were used in some sections as negative controls. Slides were mounted in Fluoromount-G (Electron Microscopy Sciences) after 3 washes in PBS. Signals were viewed using a Zeiss LSM 510 confocal microscope.

Scanning electron microscopy (SEM)

Sizes, numbers and detailed locations of otoconia were determined by SEM. Briefly, animals were anesthetized using a sub-lethal dose of ketamine (167 mg/kg) and xylazine (2 mg/kg) and perfused through the left ventricle with 0.1 M sodium cacodylate (pH7.2) followed by 20-30 ml 4% paraformaldehyde + 2.5% glutaraldehyde + 3 mM $CaCl_2$ in 0.1 M sodium cacodylate (pH7.2). Utricles and saccules were dissected out of the inner ear in the fixative and openings were made by gently breaking the bony capsules at the “roof” of the utricle and saccule. Tissues were further immersion-fixed for 24 hours in the same fixative, washed three times and post-fixed in 1% osmium tetroxide in 0.1 M sodium cacodylate (pH7.2) for 1 hour. Samples were then dehydrated, critical point dried in CO_2, mounted, sputter coated with gold palladium and viewed on a Jeol (JSM-848) scanning electron microscope at 5 kV.

Transmission electron microscopy (TEM)

Inner ear tissues were dissected out from perfused mice and fixed in 3% glutaraldehyde in 0.1 M sodium cacodylate (pH7.2) for 1 hour at 4°C. After three washes in 0.1 M Sorensen’s phosphate buffer, samples were post-fixed with 1% osmium tetroxide for 1 hour and rinsed three times in Sorensen’s buffer. Tissues were dehydrated in graded ethanol and infiltrated in 50% propylene oxide + 50% resin for 1 hour, then placed in resin for another hour, and embedded in resin-based mold for polymerization overnight in 37°C oven. Ultra-thin sections (85 nm) were taken from each sample and analyzed on a Jeol (JEM-1011) transmission electron microscope at 60 kV.

Semi-quantitative RT-PCR

Inner ear tissues were collected, total RNA was extracted using the Trizol reagent (GibcoBRL) and treated with DNase. Three micrograms of total RNA from each sample was reverse-transcribed using a New England BioLabs Reverse Transcription kit. Equal amounts of cDNA were amplified by multiplex PCR using 20 pM primers from PLA2L domain 1 that was deleted (primers are denoted by filled block arrows in Figure 1A) (5'-TTTGAGATGGAAGGGATGCCTGTG-3' and 5'-GGCAGAAGGAAGCATCCAGGAAGT-3') and 2 (5'-TACGGCTGCTACTGTGGAAGAGAAGG-3' and 5'-ATTTGGCCATGTGGTCTTAACATACC-3'). Primers (0.45 pM) from GAPDH (glyceraldehyde-3-phosphate dehydrogenase) (5'-TATGACTCCACTCACGGCAAATTCAAC–3' and 5'-AGGAGACAACCTGGTCCTCAGTGTAGC-3') were included in the same reaction as the internal standard as well as the positive control for PCR reactions. Lower concentrations of GAPDH primers were used because the gene has a much higher level of expression. PCR conditions (including primer, dNTP and Mg^{2+} concentrations and annealing temperature) were optimized and several cycle numbers (28×, 30× and 35×) were tested to ensure accurate representation of expression ratios by the semi-quantitative PCR analysis.

Assaying for total protein content and protein concentrations

Protein concentrations were measured using a Micro-BCA (bicinchoninic acid) Protein Assay Kit (Pierce) following the manufacturer's protocol. Briefly, 100μl of each diluted BSA standards and protein samples were added into microplate wells; 100μl of freshly prepared working reagent (A:B:C @ 25:24:1) was added into each well and mixed gently. The reaction was incubated at 37°C for 2 hours with rocking, and the absorbance was measured at 562 nm on a Quant MQX200 plate reader (Bio-Tek Instruments, Inc.). Sample protein concentrations were calculated according to standard curves.

Western blotting

Dissected otoconia from fresh, unfixed utricles and saccules were pooled, washed and cleaned of filaments/membranes as described below. Twenty microliters of lysis buffer (40 mM Tris, 4% CHAPS, 8 M urea, 10 mg/ml DTT, 0.15 M EDTA) was added into each sample and kept at 4°C overnight to decalcify. EDTA, buffer and salts were removed by passing through Centricon columns (Millipore) after 20-fold dilutions. The total protein concentration of each sample was measured using a Micro-BCA kit (Pierce). An aliquot of each sample containing an equal amount of total protein was mixed with 2X sample loading buffer (0.13 M Tris-HCl, 20% Glycerol, 46 mg/ml SDS, 0.2 mg/ml bromophenol blue, 20 mg/ml DTT), boiled for 5 minutes, loaded onto a 4-20% gradient Tris-SDS gel (Jule Inc.), electrophoresed at 200 V in running buffer (25 mM Tris pH8.3, 192 mM glycine, 0.1% SDS) for 4 hours, and transferred to a PVDF membrane (Millipore) at 100V for 1 hour. The blot was washed once with TBST buffer (50 mM Tris, 150 mM NaCl, 0.1% Tween-20) and treated with 3% blocking buffer (Roche Applied Science) overnight at room temperature. The membrane was incubated with primary antibodies at optimized dilutions for 3 hours followed by 3 washes in TBST buffer, and incubated with a specific peroxidase-conjugated secondary antibody (Sigma) for another 3 hours. After 3 washes, detection solution was added for 1 minute, and the blot was exposed to a Kodak X-ray film. Some membranes were stripped in 25 mM glycine-HCl (pH2) containing 1% (w/v) SDS and re-used for detection with several antibodies against different proteins.

Otoconia dissection and protein identification

Fresh, unfixed inner ear tissues were removed from the temporal bones, and utricles and saccules were separated after removal of surrounding bony structures. Otoconia were dissected from the utricle and saccule of Oc90 mutant mouse lines (wt and null) and inbred mice with Dumont-55 fine forceps (World Precision Instrument). Dissection was carried out in a Petri dish containing 0.1% NaAc (pH7.4), and the attached membranes were carefully removed from otoconia first with forceps, then by gentle rocking in 0.1% SDS/NaAc buffer (pH7.4) in a Petri dish to wash away any residual filaments or membrane debris. The crystals in a Petri dish were examined under a light microscope at high magnification (640×, Figure S1) to confirm the absence of any visible membranes and filaments before proceeding further. We do not use centrifugation for separation in these steps as it would spin down the membranes and debris. The crystals were then aspirated into a clean tube using a micropipette. Otoconia were further washed in 0.1% SDS/NaAc buffer (pH7.4), and cleaned of any possible remnants of surface filaments and residual membranes by sonication, gentle rocking and aspiration. Only then centrifugation was used to remove excess liquid and the crystal pellet was decalcified and proteins were extracted with 10μl of buffer (40 mM Tris, 4% CHAPS, 8 M urea, 10 mg/ml DTT, 0.15 M EDTA) at 4°C overnight. The buffer was used in an attempt to identify any EDTA-insoluble component of otoconia crystals as was reported for fish otolith crystals (Murayama et al., 2004).

After removal of EDTA, buffer and salts using a Centricon column (Millipore), the decalcified and denatured otoconial proteins from 30 C57Bl/6J mice were digested with 2μg trypsin/60μg otoconial protein in 50 mM Tris-HCl (pH8.6) overnight at 37°C for protein identification. The resultant peptides were determined in a single run by 75μm LD microcapillary reverse-phase high-performance liquid chromatography (HPLC) that is directly coupled to a ThermoFinnigan LCQ DECA quadruple ion trap mass spectrometer equipped with a custom nanoelectrospray source at the Harvard Microchemistry Facility. MS/MS spectra were acquired with a relative collision energy of 30% and an isolation width of 2.5 Da. The recurring ions were dynamically excluded. Interpretation of the resulting spectra was facilitated by using the program Fuzzylons developed in the above core facility and by database correlation with the algorithm SEQUEST. The sequence data were re-analyzed manually to confirm/refute the automatic analysis.

As specified in figure legends and the Results section, antibodies were either purchased (fetuin-A from R&D) or generated against either the N- or C- terminal region of otoconial proteins (Chemicon), affinity-purified on a peptide-column, and validated by Western blotting of extracts from otoconia crystals and inner ear tissues. Peptides used in immunization were synthesized and conjugated to maleimide-activated keyhole lympet hemocyanin before injection into rabbits by Chemicon. The identified otoconial proteins were further confirmed by localization in the otoconia crystals and the utricle and saccule using both Western blotting and immunostaining. The Oc90 antibody, raised against the N-terminal peptide (HALDTPNPQELPPGL) of the secreted protein, showed the same tissue distribution and Western blotting pattern as an aliquot kindly provided by Drs. Ruediger and Isolde Thalmann (Ignatova et al., 2004).

X-ray powder diffraction

As otoconia contain a number of crystallites, X-ray powder diffraction, instead of single crystal diffraction, was employed to determine the crystalline structure of Oc90 null otoconia. Diffraction was kindly performed by Mr. Peter White at the X-Ray Diffraction Facility at the University of North Carolina at Chapel Hill. Samples were mounted on MiteGen polyimide film mounts using a minimal amount of paratone-N oil. Data were collected on a Bruker-AXS SMART diffractometer equipped with graphite monochromated Cu radiation and an APEX-

II CCD detector. For each sample, a series of frames were taken at increments of 10 degrees 2θ while rotating φ. The frames were then merged using the PhaseID module of the Bruker-AXS control program and the resulting pattern was integrated to produce a powder diffraction pattern.

Results

Oc90 is essential for formation of the otoconial organic matrix that controls crystal growth and morphology

Neither Oc90 nor Oc22 is speculated to be a sPLA2 enzyme due to the substitution of several amino acids essential for the catalytic activity. Indeed, Oc22 did not show any PLA2 activity (Pote et al., 1993). However, the protein seems to have preserved the Ca^{2+}-binding properties of sPLA2, as rat Oc90 was found to bind Ca^{2+} (Pote et al., 1993). This feature may be critical for the protein to incorporate Ca^{2+} or $CaCO_3$ into the organic matrix of otoconia seeds in the Ca^{2+}-poor endolymph. We intended to test this hypothesis by examining the role of Oc90 in otoconia calcification using a gene targeting strategy. The construct design is depicted in Figure 1A.

Chimeric mice were examined for the presence of Oc90 null allele using PCR analysis of tail DNA, and null allele-carrier chimeric males were bred to C57Bl6/J females. The subsequent F_1 mice were intercrossed. The genotypes of most F_1 parents and more than half of the initial F_2 pups were confirmed by Southern blotting (Figure 1D, *Alw*N I digestion) to validate the multiplex PCR genotyping (Figure 1C, genotyping PCR primers are denoted by unfilled block arrows in 1A). In Figure 1D, the 12 kb fragment was from the wt allele and the 5.5 kb fragment from the null allele after *Alw*N I digestion of tail genomic DNA. Inactivation of Oc90 transcript (Figure 1E) and protein (Figure 4E) was demonstrated by multiplex RT-PCR of inner ear tissues and by Western blotting of otoconia crystals from 1-month-old mice, respectively. The Oc90 primers used in RT-PCR were located in the deleted region of PLA2L domain 1 (RT-PCR primers are denoted by filled block arrows in Figure 1A), and the antibody used for Western blotting was raised against the N-terminal peptide of the secreted protein (see Methods). The wt otoconia had a predominant band at 75-80 kD, as previously reported (Ignatova et al., 2004). The upper band at 180-200 kD was also seen in the report. In contrast, Oc90 null otoconia had no protein bands analyzed on the same membrane and under the same conditions. The mutant Oc90 protein is predicted to be 6.6 kD and 50 aa long (38 wt N-terminal aa +12 mutant aa), which would have migrated out of the analysis gel assuming the mutant protein was translated and stable. The same membrane detected positive for the presence of other minor otoconins (see below and Figure 4E). The smear in wt otoconia is typical of Oc90 due to the abundance of the protein and the variable degrees of glycosylation.

Confirmed nulls mice were backcrossed to the parental strain C57Bl6/J. Phenotypes were initially examined in the null, heterozygous (het) and wildtype (wt) mice generated from F_2 and F_3 heterozygous mating and were subsequently confirmed in these genotypes generated from heterozygous mating of backcrossed mice.

Examination of the vestibular histology in Oc90 null and littermate control mice showed grossly abnormal otoconia in Oc90 null mice (Figures 2 and 3). The utricle and saccule had giant “otoconia” that were transparent under a light microscope and had prominent dark deposits that are likely accumulated minerals (arrows in Figure 2C, D). These giant otoconia are apparently aggregates of numerous crystals. In contrast, crystals in wt and het mice appeared opaque under a light microscope and did not have the dark deposits. At high magnification (1,000}), these multiple crystallites were clearly visible in the mutant otoconia and all aggregated into one (Figure 2G), although occasionally there were smaller ones too in other animals examined. In Toluidine Blue stained semi-thin sections (0.5μm), the giant otoconia

from E17.5 Oc90 null embryos were composed of numerous naked crystallites without the surrounding organic matrix to divide them (Figure 2G). In contrast, the wt immature otoconial crystallites (arrows in Figure 2F) were embedded in a dark-stained organic matrix (denoted by thin arrows in Figure 2F, H). There were sometimes traces of matrix left among the null crystallites that is possibly some remaining proteoglycans. Of note, these embedded wt crystallites are different than the matrix vesicles (arrowhead in Figure 2F). These vesicles appeared to contain organic particles that stained intensely with Toluidine Blue, suggesting that they may provide some of the organic components (glycoprotein and proteoglycan). Such organic particles may become incorporated into the developing otoconia seeds as shown by white arrowheads and the inset in Figure 2H. It is possible that the organic particles may take up Ca^{2+} and $HCO3^{-}$ that are extruded by hair bundles for $CaCO_3$ deposition (also see Discussion).

During embryonic stages, each wt otoconium contained only one to several crystallites (Inset in Figure 2F), but in adults the number of crystallites increased to an estimate of 10-30. This number is still much less than in the Oc90 null otoconia. Otoconia continued to grow from E17.5 until one week postnatally. As shown in the inset of Figure 2F, there were occasional mature otoconia in the E17.5 utricle and saccule that resembled the adult otoconia in Figure 2I. These mature otoconia had most of the organic matrix centrally located, and the inorganic crystallites peripherally arranged and separated by some organic matrix. From the matrix distribution pattern, it is apparent that these individual crystallites fuse to give rise to the mature otoconia (several fused crystallites are shown in inset in Figure 2F). After merging, the embedding organic matrix of seeds now divides these crystallites. The adult vestibule had occasional otoconia seeds that are embedded in the organic matrix (thin arrow in Figure 2I), which likely arise from neogenesis. The driving force for such fusion of crystallites is likely the same as that governing the specific formation of the organic matrix: protein-protein interactions between the matrix components (Oc90-proteoglycan-otolin), which is addressed in the protein analysis section below and further postulated in Discussion based on findings from other fields regarding structurally similar molecules.

The absence (or near absence) of the organic matrix in Oc90 null otoconia apparently led to the uninhibited crystal growth similar to the growth of calcitic crystals seen in nature. The appearance of the uneven accumulation of minerals toward the center of the crystals (arrows in Figure 2C, D) is likely due to the absence of the organic matrix. This, and the transparent feature of the giant otoconia, indicates a possible lack of protein or low amount of protein in the mutant crystals of Oc90 null mice. Indeed, a micro-BCA (bicinchoninic acid) protein assay measured only approximately 31% of protein content in the null otoconia compared to equal mass of wt ones. Due to the low level of protein in null otoconia, a single micro-BCA assay required 24 null mice, making it impractical to perform multiple assays to obtain standard deviations. In the absence of the matrix, there was ~50% reduction in the overall otoconia calcification, as measured by the average mass of the null versus wt otoconia. There was occasional (1 out of 6 utricles) absent otoconia in Oc90 null mice in all age groups including E17.5 null embryos. Thus, the organic matrix plays a double role. First, it efficiently recruits the inorganic particles and/or stabilizes them. Second, it provides a framework that guides the growth of $CaCO_3$ particles, as indicated by the irregular morphology of the null otoconia.

Compared to wt otoconia, the null otoconia did not adhere as securely to the membranous honeycomb layer that lies underneath the crystal layer above the sensory epithelium. Indeed, the mutant otoconia in more than 75% of Oc90 null mice were loose. The loose otoconia were occasionally displaced into the semi-circular canals or become associated with the "roof" (Figure 2E). The clinical condition benign paroxysomal positional vertigo (BPPV), the most common form of dizziness, is caused by loose otoconia that fall into the posterior and sometimes horizontal canal. Some giant otoconia in Oc90 null mice that were attached to the

"roof" of the saccule and utricle may be a defect in transporting the crystal seeds from the squamous non-sensory epithelium ("roof") to the sensory epithelium. Such "roof" localization of inorganic mutant crystals was also seen in morphant zebrafish for otopetrin (Hughes et al., 2004). The "roof" of the utricle and saccule has the potential to form organic matrix of the crystals due to its expression of Oc90 (Verpy et al., 1999;Wang et al., 1998) and OMP in fish (Murayama et al., 2004). Indeed, fibrous organic matrix was seen attached to the roof of the saccule in the *hslt* and otogelin mutant mice (Kiss et al., 2006) and fish (Murayama et al., 2004). The loose otoconia in the absence of Oc90 suggest that either Oc90 or the organic matrix may provide some adhesion of the crystals to the otoconial membrane. The sheer size of the null otoconia may have also contributed to the detachment.

Scanning electron microscopy (SEM) showed that these crystals were approximately 20-500 times larger than wt ones (Figure 3A-D). Averaged measurements of lengths and mid-section width are shown in Table 1. The giant null crystals had surface folds resembling "rock formations" often seen in nature. The morphological distortion was worse in the utricle than the saccule. Otoconia in het mice appeared to be normal under both the light microscope and SEM (data not shown). The wt crystals averaged ~24μm in length and ~13μm in width for the ones above the peripheral utricular macula and ~16μm in length and ~7μm in width for the ones above the central utricular macula. The saccular otoconia were much smaller, measuring ~4μm in length and ~2μm in width. The ratio of length versus width was about 2:1 and the shape of each otoconial crystal was hexagonal cylindrical with pointed ends although the size may vary. However, Oc90 null otoconia had irregular shapes. The length ranged from 100μm to 300μm; the ratio of length versus width ranged from 1.5:1 to 5:1. The number, size and shape of null otoconia varied dramatically from animal to animal in both the utricle and saccule. On average, 1-month-old null mice had 7±5 giant crystals in the utricle and 9±6 in the saccule (n=42 ears). There was asymmetry in the number and size of the giant otoconia in the left and right ears, but the difference did not reach statistical significance.

X-ray powder diffraction showed that these mutant otoconia in Oc90 null mice had the same calcitic crystalline structure as wt and het otoconia (Figure 3E, 3 months old), as were the reported star-shaped otolith aggregates in morphant zebrafish for starmaker (Sollner et al., 2003) and the inorganic otoliths in morphant zebrafish for otopetrin (Hughes et al., 2004). As shown in Figure 2D, the gross morphology of Oc90 null otoconia resembles these reported star-shaped calcite crystals as well. "Crystalline structure" is the organization of the molecular lattice, and "otoconia morphology" refers to the microscopic appearance of each otoconium. In Figure 3E, a series of frames were taken at increments of 10 degrees 2θ while rotating φ for each sample. The frames were then merged to give the peak patterns. The patterns of peak positions for wt, het and null otoconia in Figure 3E are all consistent with the calcitic *R-3c* of $CaCO_3$ (Effenberger H et al., 1981). The variations in peak heights between wt, het and null crystals are indications of their high degree of preferred orientation (or their distinct crystal shapes). The unchanged calcitic pattern of Oc90 null otoconia demonstrates that the organic matrix does not influence the inorganic crystalline structure.

Given the young age (P20) of the Oc90 null animals examined initially, the observed giant otoconia likely arose from abnormal development. To further confirm this, we examined additional mutant otoconia at earlier stages of embryonic development including E16.5 and E17.5 (E16.5 is shown in Figure 5J and 7B, 7D). At these stages, wt otoconia are still being seeded (E16.5) or seeding is just near completion (E17.5). The crystals in Oc90 null mice at both stages were also giant aggregates. Thus, the giant otoconia were indeed a consequence of embryonic malformation.

These sets of data demonstrate that Oc90 is required to form the organic matrix and this matrix controls otoconia growth and morphology and provides maximum calcification efficiency. The

Ca^{2+}-binding capabilities of Oc90 and proteoglycans (known matrix components) may efficiently recruit the micro-environmental Ca^{2+} near the macula for optimal $CaCO_3$ deposition.

Oc90 recruits otolin to form the organic matrix of otoconia

Absence of the entire organic matrix in Oc90 null otoconia led us to hypothesize that Oc90 recruits other otoconin and/or organic components to form this organic matrix. The onset of Oc90 expression is around E9.5 (Verpy et al., 1999), days before the first appearance of any detectable otoconia seeds (around E15) (Anniko, 1980;Takumida and Harada, 1984), further indicating such possibility. To test the hypothesis, we began an effort to identify the low-abundance otoconins that have remained elusive in the past due to difficulties in obtaining sufficient quantity. The current availability of ultra-sensitive proteomic technologies has made this task feasible. To extract all types of otoconins, we used both EDTA (0.15 M, pH8.0) and CHAPS (4%) to decalcify the crystals, as fish otoliths contain both EDTA-soluble (otolith matrix protein or OMP) and EDTA-insoluble (otolin) components. Both mouse otoconia and fish otoliths have internal fibrous structures, albeit much finer in the former. These fibrous structures are made of otolin in otoliths (Murayama et al., 2004).

In addition to the abundant Oc90 that was identified previously (Verpy et al., 1999;Wang et al., 1998), we successfully identified and validated two proteins, otolin (aka otolin-1) and fetuin-A, to be components of murine otoconia crystals (for accession numbers see Table 2). We subsequently generated antibodies and confirmed this finding by Western blotting of protein extracts from dissected crystals (Figure 4E), immunostaining and RT-PCR (described below). BLAST search of mouse genome indeed showed a murine ortholog of fish otolin. Previous failure to identify this protein in mammalian otoconia was likely caused by the extraction methods, which only used EDTA.

An antibody against murine otolin was raised in rabbit against the C-terminal unique peptide FSGFLLYPEETFSKSP. Validation of this antibody was carried out first by Western blotting of extracts from wt otoconial crystals and inner ear epithelium (Figure 4E). Analysis with the wt inner ear epithelium produced a single band of 60 kD, slightly larger than the predicted 49.6 kD possibly due to glycosylation. Fish otolin is even larger (around 100 kD) (Murayama et al., 2002) than its predicted size (45.6 kD) because of glycosylation, dimerization or both. In the wt otoconia crystals, Western blotting showed multiple bands (Figure 4E), which is likely caused by formation of extra-cellular multimers similar to its family member collagen X. Apparently, the 10 mg/ml DTT used could not break completely the multimers. Notably, otolin was absent (or below the detection level) in Oc90 null crystals, whereas fetuin-A and osteopontin were present (Figure 4E). The same membrane used for Oc90 analysis was stripped and re-used for detection of fetuin-A (55 kD) and osteopontin (50 kD) with monoclonal antibodies (supplied by R&D) in Figure 4E. All otoconins were present in wt crystals (Figure 4E). Approximately 3.7μg of wt and 5.1μg of null otoconia protein were loaded. As null otoconia are largely inorganic, equal amounts of null otoconial proteins (total protein content) are expected to contain significantly more minor otoconins than wt otoconia, therefore the null otoconia had seemingly more fetuin-A and osteopontin proteins. These sets of data suggest that Oc90 specifically recruits otolin to form the organic matrix of otoconia.

Otolin had a low level of expression in the transitional epithelial cells of the utricle and saccule in wt mice as detected by fluorescent immunostaining using the C-terminal-directed antibody (the utricle is shown in Figure 4A, B; several otolin-positive transitional cells are denoted by unfilled arrowheads in Figure 4A). The expression in the transitional epithelium was not as visible in the E16.5 mouse utricle and saccule. Similarly, fish otolin expression was more obvious in the adult transitional epithelium of the utricle and saccule than embryonic stages although the protein was present in otolith seeds on E15 (Murayama et al., 2002). Notably, a

low level of otolin protein was also detected in the otoconial membrane (OM) (arrows in Figure 4A) and the pericellular matrix of the macular epithelial cells, including hair cells (block arrow in Figure 4A) and supporting cells (filled arrowheads in Figure 4A), in the wt mouse vestibule. In contrast, it was not detectable in the OM or luminal surface of the Oc90 null utricle and saccule (Figure 4B). The overall staining intensity in the macula and the transitional epithelium of the null sections (Figure 4B) was consistently much lower than that in the wt vestibule of both E16.5 and P20 age groups (P20 is shown), with only faint signals in the matrix facing the basement membrane of the null utricle and saccule (filled arrowheads in Figure 4B). Semi-quantitative multiplex RT-PCR showed positive transcription of otolin in Oc90 null and wt inner ear epithelial tissues (Figure 4C, 1 month old). Being expressed in the squamous cells, Oc90 is not likely to have affected the transcription of otolin. Therefore, Oc90 induces the recruitment and accumulation of otolin in otoconia crystals, OM and the luminal extra-cellular matrix. Similarly, fish OMP was found to recruit otolin (Murayama et al., 2005). Fish otolin protein was only detected in the few transitional epithelial cells (Murayama et al., 2004), likely due to the lower sensitivity of color reactions used in the study. The pericellular distribution pattern of otolin in the inner ear is similar to that of collagen X in hypertrophic chondrocytes (Kwan et al., 1991;Sawada et al., 1990). There was no increase in the intracellular otolin accumulation in the Oc90 null vestibule, indicating that Oc90 more likely affected the extra-cellular deposition of otolin and not its secretion. The structurally similar molecule sPLA2 also induces collagen deposition in the vascular wall via an unknown mechanism (Ghesquiere et al., 2005).

If Oc90 indeed recruits otolin to form the organic matrix, one would expect to see the presence of otolin during wt otoconia seeding. We examined otoconia seeds on E16.5 for the presence of these otoconins (immunostaining) and $CaCO_3$ (Alizarin red complexone, ARC). Fluorescent immunostaining showed a high level of Oc90 (Figure 5A) and a low level of otolin (Figure 5E) (but no fetuin-A) in wt otoconia seeds on E16.5. The onset of otolin expression began around E15.5-E16.5. The later onset of otolin expression, as compared to that for Oc90 (or OMP in fish), and the absence (or great reduction) of otolin in Oc90 null crystals, suggest that Oc90 recruits otolin, as does OMP in fish (Murayama et al., 2005), to form an organic matrix upon which the crystals are calcified.

Despite the appearance of otoconia seeds (Figure 5A, C, E, G), sections of the E16.5 wt utricle or saccule did not contain any detectable $CaCO_3$, whereas adjacent bones and cartilages were stained (Figure 5D; stained tibia is shown in the inset). Whole-mount utricles and saccules from E16.5 wt mice did not show stained seeds either (Figure 5I), but null tissues stained positive (Figure 5J), likely due to the aggregation of the crystallites that increased the sizes of the particles and the amount of $CaCO_3$ available for positive detection. Observation of E16.5 otoconia seeds showed that the aggregation of crystallites in Oc90 null mice began early during development. Also, the naked crystallites in the null otoconia may be providing ready access by the dye in the whole mount staining. P0 whole mount wt otoconia stained robustly with this fluorescent dye (Figure 5H, utricle is shown). These sets of data suggest that formation of the organic matrix precedes the deposition of $CaCO_3$ crystallites. The matrix likely provides a framework for $CaCO_3$ deposition.

Expression of fetuin-A was not detectable in the inner ear epithelium by immunostaining, RNA *in situ* hybridization or RT-PCR (Figure 4D). Its presence in otoconia crystals was validated by Western blotting (Figure 4E), and the transcript was detected in the brain (Figure 4D). Thus, fetuin-A protein does not originate from the vestibular epithelium and may have been incorporated into otoconia from the endolymph. Fetuin-A is known to be abundantly transcribed in the liver and resides mostly in the serum and calcified bone.

Mass spectrometry analysis did not detect osteopontin, although the presence of the protein in otoconia was previously detected by immunostaining (Takemura et al., 1994). This implies that either the level of osteopontin is extremely low, or the protein is not an intrinsic crystal component but only adheres to the crystals and was washed away by our vigorous washes. Presence of these bone matrix proteins (osteopontin and fetuin-A) and matrix analogous proteins (otolin) in otoconia strongly suggests mechanistic similarities between otoconia and bone calcification.

Oc90 null mice have reduced acellular structures but normal gross morphology of the inner ear

Interestingly, in addition to reduced otoconia, the utricle and saccule also had otoconial membranes that appeared to be brittle, less compact and frequently broken with the more delicate fibers in the honeycomb layer (Figure 6B, D). There were flora-like membranes (inset in Figure 6D), which were also observed in the *hslt* (NoxO1) mice (Kiss et al., 2006). Oc90 protein was detected in the P20 wt otoconial membrane (OM, arrows in Figure 6E), in addition to the crystals (arrowhead in Figure 6E), in partially decalcified sections, which was not reported before. The protein was absent in this membrane in the null mice (arrows in Figure 6F inset show phalloidin-stained OM). However, it is likely that a combination of absent Oc90 and greatly reduced otolin in the OM caused the fragile appearance of the membrane in Figure 6B and 6D.

The cupula and tectorial membranes (TM) were also thinner in Oc90 null mice (Figure 7E-H). The average thickness of the E16.5 cupula was 32.5±2.5μm for wt and 15.7±2.6μm (n=6, $p<0.0001$) for null mice, and the average midway thickness of the TM was 21.0±0.6μm for wt and 6.7±0.6μm (n=6, $p<0.0001$) for null mice (9 months old sampled for TM measurements). Fluorescent immunostaining showed abundant Oc90 protein in the P20 wt but not null cupula (Figure 8E, F). Despite a previous report of a weak Oc90 signal in the postnatal TM (Verpy et al., 1999), we did not detect any signal in this matrix in either embryonic or P20 wt tissues (negative staining of P20 wt TM is shown as inset in Figure 8E). These acellular matrices also bind Ca^{2+} (Kawamata, 1991) and can become calcified under pathological conditions (Johnsson et al., 1981;Johnsson et al., 1982). Additionally, the null TM stained more intensely with Toluidine Blue (inset of Figure 7H), likely caused by a condensation of collagens. The acellular matrix (arrows in Figure 7G, H) adjacent to the inner hair cell in the E16.5 cochlea that gives rise to the future TM was also significantly thinner. The vestibular functional consequence of a thinner cupula is presently unclear, as no study has been done to examine the influence of the otoconial membrane or the cupula on mechanotransduction of the vestibular hair cells or on an animal's balance behavior. The reduction of these acellular structures in the absence of Oc90 shows that the protein may also play a role, albeit non-essential, in organizing these structures.

Despite the abundant Oc90 expression in the non-sensory epithelium of the inner ear (Verpy et al., 1999;Wang et al., 1998), the null mice had apparently normal cellular structures in H & E (hematoxylin and eosin) stained inner ear sections (E16.5 shown in Figure 7). All epithelial cells, including hair/supporting cells, marginal zone/transitional epithelium and squamous cells, appeared to be normal morphologically (Figure 7) and ultrastructurally (Figure 8C, D, 9 month-old saccule is shown). On E16.5, the null utricle and saccule had only several large otoconia particles (arrows in Figure 7B, D), as compared with the normal minute seeds in the wt vestibule (Figure 7A, C). There were greatly reduced otoconial membranes (labeled OM in Figure 7D) in the null vestibule, which stained much lighter for H&E due to the reduction of glycoproteins and proteoglycans. The stereocilia density and organization were also normal as demonstrated by phalloidin staining (Figure 8A, B).

Discussion

We show in this study that Oc90 is required for formation of the organic matrix of otoconia. Without this matrix, the inorganic crystallites have the propensity to grow uninhibitedly, as seen with calcite crystals (inorganic $CaCO_3$) in nature. This is strikingly similar to bone crystals, whose growth is also controlled by cross-linked bone matrix proteins. Indeed, the matrix vesicles we observed show great resemblance to those in bone. Both otoconins and bone matrix proteins are extremely acidic with highly enriched negative charges. Such an acidic feature provides the molecules an affinity for calcite and apatite. Bone mineralization is thought to occur in two phases: initially via matrix vesicles for the formation of hydroxyapatite, and later through nucleation at collagen fibrils for the proliferation of mineral crystals within the extra-celluar matrix (ECM) (Anderson, 1995;Christoffersen and Landis, 1991). Similar to collagen and/or bone matrix proteins (Landis, 1995), our study shows that the organic matrix in otoconia provides a framework that determines the correct orientation, sizes and shapes of crystals.

In bone, pericellular collagen X of hypertrophic chondrocytes is associated with the deposition of fibrillar collagens for endochondral calcification (Chan and Jacenko, 1998), whereas the matrix form of collagen X in cell culture forms a hexagonal lattice (Kwan et al., 1991;Sawada et al., 1990). The fibrous structure in the TEM sections of wt otoconia is likely oligomerized otolin, as demonstrated by Western blotting in Figure 4E. The pericellular distribution of otolin in the macula and formation of multimers in otoconia suggest that otolin likely plays a similar role in $CaCO_3$ deposition. The reduction in otolin accumulation in the Oc90 null vestibule may have contributed partially to the reduced otoconia calcification. Interestingly, our preliminary observations show that Oc90 is also expressed in hypertrophic chrondrocytes, in addition to its presence in the calcified bone matrix and osteocytes, suggesting that Oc90 may play a role in collagen deposition in bone as well and further indicating that otoconia and bone calcification share some common mechanistic features.

However, there are fundamental differences between bone and otoconia calcification, primarily due to the low Ca^{2+} in the endolymph and the unique features of the mechanosensory hair/supporting cells in the inner ear. For example, the Ca^{2+} for otoconia calcification is primarily extruded by PMCA2, as deletion of the type 2 isoform alone leads to a complete absence of otoconia (Kozel et al., 1998). This suggests that $CaCO_3$ is formed extra-cellularly after extrusion of Ca^{2+} and HCO_3^- by hair cells. Severe to absent otoconia abnormalities occur when non-component ions are perturbed in the endolymph (i.e., Na^+, K^+, Cl^-) (Blasiole et al., 2006;Everett et al., 2001). Null deletion of the Cl^-/I^- transporter (aka $Cl^-/HCO3^-$ exchanger) pendrin (Pds) causes absent to greatly reduced otoconia (Everett et al., 2001). The effect of the transporter on otoconia formation is likely through extrusion of HCO_3^- (Royaux et al., 2001). It can also affect the pH via dysregulated HCO_3^- (Stankovic et al., 1997), which subsequently affects the stable maintenance of $CaCO_3$ crystal seeds. All these lines of evidence suggest that the Ca^{2+} and $HCO3^-$ are primarily provided by ion pump/channel activities. Although our current study does not provide direct evidence as to where $CaCO_3$ is initially deposited (as our current focus is the formation of the organic matrix), when interpreted with the above reports, our finding that the organic matrix is formed prior to the deposition of inorganic $CaCO_3$ calls for modification of the earlier belief that otoconia are formed from preotoconium particles released from large vesicular bodies secreted by macular cells (Anniko, 1980;Harada, 1979;Nakahara and Bevelander, 1979;Takumida and Harada, 1984).

It is not clear if the matrix vesicles we observed are the “globular substances”, or large secretory vesicles or blebs, that were previously reported by other investigators (Anniko, 1980;Suzuki et al., 1995). However, these secretory blebs are not unique to the macula of the inner ear. Blebs of exactly the same appearances are seen in cochlear inner hair cells (Shi et al., 2005).

Additionally, they are abundant in the adult vestibule, a time when otoconia formation is completed. As higher osmolarity inhibited formation of these blebs, it is likely that at least a certain percentage of these blebs are artifacts caused by a change in the ionic composition of the buffer as compared to the *in vivo* endolymph. It is unclear whether and to what degree these vesicles may provide additional Ca^{2+} (Suzuki et al., 1995) *in vivo* and whether they secrete some otoconia and membrane components, such as otopetrin, a-tectorin and otogelin. Otopetrin is responsible for the secretion of a zebrafish otolith protein starmaker (Sollner et al., 2004) and is postulated to be involved in intra-cellular vesicular transportation that may be related to the secretory blebs (Hughes et al., 2006). The exact roles of these proteins in $CaCO_3$ formation have not been defined. It is possible that Ca^{2+} and $HCO3^-$ may be taken up by the secretory vesicles upon extrusion and the two pathways (ion extrusion and otoconin secretion) converge. However, no evidence exists to demonstrate such vesicular uptake of ions. Additionally, secretion alone cannot explain the specific accumulation of a few proteins in the otoconia matrix. Such specificity is likely rendered through protein-protein interactions.

Absence of the entire organic matrix in Oc90 null otoconia suggests that Oc90, otolin and proteoglycans specifically interact with each other to form this matrix. Other non-ECM minor otoconins, such as fetuin-A and osteopontin, are not affected in the Oc90 null mice. The specific recruitment of otolin by Oc90 may arise from the mutual affinity of Oc90 and otolin for proteoglycans. Otolin has a collagen X and C1q domain, and both domains have a high affinity for proteoglycans and Ca^{2+} and affect secretion/endocytosis (Groeneveld et al., 2005). Oc90 shows some of the inactive sPLA2 activities due to the great degree of similarities between their secondary structures (Pote et al., 1993). Thus, Oc90 may also bind proteoglycans, which are present both in the otoconial crystals and membranes (Fermin et al., 1990;Sartipy et al., 1999;Sartipy et al., 1998). This may explain the loose otoconia in Oc90 null mice. Otolin may also interact with the nidogen domain of α-tectorin in the otoconial membrane for crystal anchoring. As the otoconial membrane-bound otopetrin is not present in the crystals (Hurle et al., 2003), it is not likely that Oc90 directly interacts with the protein.

We speculate that there may be a functional coupling between hair/supporting cells, which leads to a chain of events including ionic exchanging (by hair cells) and sequestration (by matrix proteins) as well as protein recruitment and endo-/exocytosis, to facilitate otoconia formation. Specifically, the PMCA2-extruded Ca^{2+} may be sequestered by Oc90-otolin-proteoglycans in and near the macular ECM. All three components have an affinity for Ca^{2+}. An added benefit of Ca^{2+}-sequestration is that it may help hair cell function by taking free Ca^{2+} away from hair bundles, as high Ca^{2+} is incompatible with hair cell function. Subsequently, this Oc90-otolin-proteoglycan-Ca^{2+} complex may induce endo-/exocytosis coupling that provides some crystal and membrane components. A rise in the extra-cellular matrix Ca^{2+} can induce synaptic vesicle coupling through an unknown mechanism (Schweizer and Ryan, 2006;Zefirov et al., 2006). sPLA2 modulates endocytosis through its high affinity for proteoglycans (Sartipy et al., 1998;Sartipy et al., 1999). In the absence of Oc90, proteoglycans in the macular ECM may sequester Ca^{2+} for CaCO3 seeding, albeit with reduced efficiency. Alternatively, fetuin-A, osteopontin and/or some other unknown minor otoconins may be sufficient to seed some of the inorganic $CaCO_3$ crystallites. However, osteopontin knockout mice have normal otoconia (Lundberg, unpublished observation). Given the low level of fetuin-A in otoconia crystals, the protein is not likely to play a major role in binding calcite crystals.

Presently it is unclear why the cupula does not mineralize even though it is abundant with Oc90. Our data show that presence/absence of Oc90 is not an indication of possibility for calcification. For example, the macula does not express Oc90 (Figure 5A), yet calcification takes place above it; the tectorial membrane does not have Oc90 (or only an extremely low level of it), yet there is no calcification under normal conditions. It is conceivable that other

factors or a combination of events are required for $CaCO_3$ to form and grow. Oc90 instead is responsible for maintaining the integrity of these acellular structures. Studies are underway to assess the functional consequence of these altered matrices. Preliminary hearing tests show that young Oc90 null mice (4 months-old) have normal hearing despite the dysmorphology of the tectorial membrane (unpublished data).

In summary, our study demonstrates that Oc90, the predominant otoconin, is the essential organizer of the otoconial matrix, and this matrix controls crystal growth and provides optimal calcification. Our data indicate that alterations in otoconial proteins may contribute to the dislocation of otoconia, which underlie the etiology for BPPV and other types of otoconia-related diseases. Our analyses of the crystal components and crystal ultra-structures suggest mechanistic similarities and differences between otoconia and bone calcification, and the differences arise from the unique features of the inner ear.

Supplementary Material

Refer to Web version on PubMed Central for supplementary material.

Acknowledgements

We thank Dr. D. M. Ornitz for support and advice during the project; Dr. J. McGee for preliminary ABR assessment of the Oc90 null mice; Dr. B. Fritzsch for technical guidance with some initial work of the SEM and initial inner ear dissection; Dr. J. Zuo for advice on the design of the knockout construct; Dr. Sherri M. Jones for editorial assistance with some parts of the text; Mr. P. White for X-ray powder diffraction; Mr. W. Lane for mass spectrometry of otoconial proteins and Drs. B. J. Morley, D. Cosgrove and W. Jesteadt for helpful discussions. Part of the work was supported by a grant from the National Center for Research Resources (1P20RR018788-01, YWL).

Reference List

Anderson HC. Molecular biology of matrix vesicles. Clin Orthop Relat Res 1995:266–280. [PubMed: 7634645]

Anniko M. Development of otoconia. Am J Otolaryngol 1980;1:400–410. [PubMed: 7457761]

Anniko M, Wenngren BI, Wroblewski R. Aberrant elemental composition of otoconia in the dancer mouse mutant with a semidominant gene causing a morphogenetic type of inner ear defect. Acta Otolaryngol 1988;106:208–212. [PubMed: 3176966]

Blasiole B, Canfield VA, Vollrath MA, Huss D, Mohideen MA, Dickman JD, Cheng KC, Fekete DM, Levenson R. Separate Na,K-ATPase genes are required for otolith formation and semicircular canal development in zebrafish. Dev Biol 2006;294:148–160. [PubMed: 16566913]

Carlstrom D. Crystallographic study of vertebrate otoliths. Biological Bulletin 1963;125:441–463.

Chan D, Jacenko O. Phenotypic and biochemical consequences of collagen X mutations in mice and humans. Matrix Biol 1998;17:169–184. [PubMed: 9707340]

Christoffersen J, Landis WJ. A contribution with review to the description of mineralization of bone and other calcified tissues in vivo. Anat Rec 1991;230:435–450. [PubMed: 1928750]

Davis JG, Burns FR, Navaratnam D, Lee AM, Ichimiya S, Oberholtzer JC, Greene MI. Identification of a structural constituent and one possible site of postembryonic formation of a teleost otolithic membrane. Proc Natl Acad Sci U S A 1997;94:707–712. [PubMed: 9012849]

Effenberger H, Mereiter K, Zemann J. Crystal structure refinements of magnesite, calcite, rhodochrosite, siderite, smithonite, and dolomite, with discussion of some aspects of the stereo-chemistry of calcite type carbonates. Z Kristallogr 1981;156:233–243.

Endo S, Sekitani T, Yamashita H, Kido T, Masumitsu Y, Ogata M, Miura M. Glycoconjugates in the otolithic organ of the developing chick embryo. Acta Otolaryngol 1991;(Suppl 481):116–120.

Everett LA, Belyantseva IA, Noben-Trauth K, Cantos R, Chen A, Thakkar SI, Hoogstraten-Miller SL, Kachar B, Wu DK, Green ED. Targeted disruption of mouse Pds provides insight about the inner-ear defects encountered in Pendred syndrome. Hum Mol Genet 2001;10:153–161. [PubMed: 11152663]

Fermin CD, Lovett AE, Igarashi M, Dunner K Jr. Immunohistochemistry and histochemistry of the inner ear gelatinous membranes and statoconia of the chick (Gallus domesticus). Acta Anat (Basel) 1990;138:75–83. [PubMed: 2368600]

Ghesquiere SA, Gijbels MJ, Anthonsen M, van Gorp PJ, van dMI, Johansen B, Hofker MH, de Winther MP. Macrophage-specific overexpression of group IIa sPLA2 increases atherosclerosis and enhances collagen deposition. J Lipid Res 2005;46:201–210. [PubMed: 15576846]

Groeneveld TW, Oroszlan M, Owens RT, Faber-Krol MC, Bakker AC, Arlaud GJ, McQuillan DJ, Kishore U, Daha MR, Roos A. Interactions of the extracellular matrix proteoglycans decorin and biglycan with C1q and collectins. J Immunol 2005;175:4715–4723. [PubMed: 16177119]

Harada Y. Formation area of the statoconia. Scan Electron Microsc 1979:963–966. [PubMed: 42971]

Hughes I, Blasiole B, Huss D, Warchol ME, Rath NP, Hurle B, Ignatova E, Dickman JD, Thalmann R, Levenson R, Ornitz DM. Otopetrin 1 is required for otolith formation in the zebrafish Danio rerio. Dev Biol 2004;276:391–402. [PubMed: 15581873]

Hughes I, Thalmann I, Thalmann R, Ornitz DM. Mixing model systems: using zebrafish and mouse inner ear mutants and other organ systems to unravel the mystery of otoconial development. Brain Res 2006;1091:58–74. [PubMed: 16529728]

Hurle B, Ignatova E, Massironi SM, Mashimo T, Rios X, Thalmann I, Thalmann R, Ornitz DM. Non-syndromic vestibular disorder with otoconial agenesis in tilted/mergulhador mice caused by mutations in otopetrin 1. Hum Mol Genet 2003;12:777–789. [PubMed: 12651873]

Ignatova EG, Thalmann I, Xu B, Ornitz DM, Thalmann R. Molecular mechanisms underlying ectopic otoconia-like particles in the endolymphatic sac of embryonic mice. Hear Res 2004;194:65–72. [PubMed: 15276677]

Ito M, Spicer SS, Schulte BA. Histochemical detection of glycogen and glycoconjugates in the inner ear with modified concanavalin A-horseradish peroxidase procedures. Histochem J 1994;26:437–446. [PubMed: 8045784]

Johnsson LG, Rouse RC, Hawkins JE Jr, Kingsley TC, Wright CG. Hereditary deafness with hydrops and anomalous calcium phosphate deposits. Am J Otolaryngol 1981;2:284–298. [PubMed: 7325303]

Johnsson LG, Rouse RC, Wright CG, Henry PJ, Hawkins JE Jr. Pathology of neuroepithelial suprastructures of the human inner ear. Am J Otolaryngol 1982;3:77–90. [PubMed: 7091544]

Jones SM, Erway LC, Bergstrom RA, Schimenti JC, Jones TA. Vestibular responses to linear acceleration are absent in otoconia-deficient C57BL/6JEi-het mice. Hear Res 1999;135:56–60. [PubMed: 10491954]

Jones SM, Erway LC, Johnson KR, Yu H, Jones TA. Gravity receptor function in mice with graded otoconial deficiencies. Hear Res 2004;191:34–40. [PubMed: 15109702]

Kawamata S. Localization of pyroantimonate-precipitable calcium in the vestibular organs of the rat and guinea pig. Arch Histol Cytol 1991;54:173–180. [PubMed: 1873075]

Kiss PJ, Knisz J, Zhang Y, Baltrusaitis J, Sigmund CD, Thalmann R, Smith RJ, Verpy E, Banfi B. Inactivation of NADPH oxidase organizer 1 Results in Severe Imbalance. Curr Biol 2006;16:208–213. [PubMed: 16431374]

Kozel PJ, Friedman RA, Erway LC, Yamoah EN, Liu LH, Riddle T, Duffy JJ, Doetschman T, Miller ML, Cardell EL, Shull GE. Balance and hearing deficits in mice with a null mutation in the gene encoding plasma membrane Ca2+-ATPase isoform 2. J Biol Chem 1998;273:18693–18696. [PubMed: 9668038]

Kwan AP, Cummings CE, Chapman JA, Grant ME. Macromolecular organization of chicken type X collagen in vitro. J Cell Biol 1991;114:597–604. [PubMed: 1860888]

Landis WJ. The strength of a calcified tissue depends in part on the molecular structure and organization of its constituent mineral crystals in their organic matrix. Bone 1995;16:533–544. [PubMed: 7654469]

Lins U, Farina M, Kurc M, Riordan G, Thalmann R, Thalmann I, Kachar B. The otoconia of the guinea pig utricle: internal structure, surface exposure, and interactions with the filament matrix. J Struct Biol 2000;131:67–78. [PubMed: 10945971]

Murayama E, Herbomel P, Kawakami A, Takeda H, Nagasawa H. Otolith matrix proteins OMP-1 and Otolin-1 are necessary for normal otolith growth and their correct anchoring onto the sensory maculae. Mech Dev 2005;122:791–803. [PubMed: 15905077]

Murayama E, Takagi Y, Nagasawa H. Immunohistochemical localization of two otolith matrix proteins in the otolith and inner ear of the rainbow trout, Oncorhynchus mykiss: comparative aspects between the adult inner ear and embryonic otocysts. Histochem Cell Biol 2004;121:155–166. [PubMed: 14689310]

Murayama E, Takagi Y, Ohira T, Davis JG, Greene MI, Nagasawa H. Fish otolith contains a unique structural protein, otolin-1. Eur J Biochem 2002;269:688–696. [PubMed: 11856329]

Nakahara H, Bevelander G. An electron microscope study of crystal calcium carbonate formation in the mouse otolith. Anat Rec 1979;193:233–241. [PubMed: 426296]

Pisam M, Jammet C, Laurent D. First steps of otolith formation of the zebrafish: role of glycogen? Cell Tissue Res 2002;310:163–168. [PubMed: 12397371]

Pote KG, Hauer CR III, Michel H, Shabanowitz J, Hunt DF, Kretsinger RH. Otoconin-22, the major protein of aragonitic frog otoconia, is a homolog of phospholipase A2. Biochemistry 1993;32:5017–5024. [PubMed: 8494877]

Pote KG, Ross MD. Each otoconia polymorph has a protein unique to that polymorph. Comp Biochem Physiol B 1991;98:287–295. [PubMed: 1873986]

Royaux IE, Wall SM, Karniski LP, Everett LA, Suzuki K, Knepper MA, Green ED. Pendrin, encoded by the Pendred syndrome gene, resides in the apical region of renal intercalated cells and mediates bicarbonate secretion. Proc Natl Acad Sci U S A 2001;98:4221–4226. [PubMed: 11274445]

Salvinelli F, Firrisi L, Casale M, Trivelli M, D'Ascanio L, Lamanna F, Greco F, Costantino S. Benign paroxysmal positional vertigo: diagnosis and treatment. Clin Ter 2004;155:395–400. [PubMed: 15700633]

Sartipy P, Bondjers G, Hurt-Camejo E. Phospholipase A2 type II binds to extracellular matrix biglycan: modulation of its activity on LDL by colocalization in glycosaminoglycan matrixes. Arterioscler Thromb Vasc Biol 1998;18:1934–1941. [PubMed: 9848887]

Sartipy P, Camejo G, Svensson L, Hurt-Camejo E. Phospholipase A(2) modification of low density lipoproteins forms small high density particles with increased affinity for proteoglycans and glycosaminoglycans. J Biol Chem 1999;274:25913–25920. [PubMed: 10464335]

Sawada H, Konomi H, Hirosawa K. Characterization of the collagen in the hexagonal lattice of Descemet's membrane: its relation to type VIII collagen. J Cell Biol 1990;110:219–227. [PubMed: 2104858]

Schweizer FE, Ryan TA. The synaptic vesicle: cycle of exocytosis and endocytosis. Curr Opin Neurobiol 2006;16:298–304. [PubMed: 16707259]

Shi X, Gillespie PG, Nuttall AL. Na+ influx triggers bleb formation on inner hair cells. Am J Physiol Cell Physiol 2005;288:C1332–C1341. [PubMed: 15689412]

Simmler MC, Cohen-Salmon M, El-Amraoui A, Guillaud L, Benichou JC, Petit C, Panthier JJ. Targeted disruption of otog results in deafness and severe imbalance. Nat Genet 2000;24:139–143. [PubMed: 10655058]

Sollner C, Burghammer M, Busch-Nentwich E, Berger J, Schwarz H, Riekel C, Nicolson T. Control of crystal size and lattice formation by starmaker in otolith biomineralization. Science 2003;302:282–286. [PubMed: 14551434]

Sollner C, Schwarz H, Geisler R, Nicolson T. Mutated otopetrin 1 affects the genesis of otoliths and the localization of Starmaker in zebrafish. Dev Genes Evol 2004;214:582–590. [PubMed: 15480759]

Squires TM, Weidman MS, Hain TC, Stone HA. A mathematical model for top-shelf vertigo: the role of sedimenting otoconia in BPPV. J Biomech 2004;37:1137–1146. [PubMed: 15212918]

Stankovic KM, Brown D, Alper SL, Adams JC. Localization of pH regulating proteins H+ATPase and Cl-/. Hear Res 1997;114:21–34. [PubMed: 9447915]

Steyger PS, Wiederhold ML. Visualization of newt aragonitic otoconial matrices using transmission electron microscopy. Hear Res 1995;92:184–191. [PubMed: 8647742]

Suzuki H, Ikeda K, Takasaka T. Biological characteristics of the globular substance in the otoconial membrane of the guinea pig. Hear Res 1995;90:212–218. [PubMed: 8974999]

Takemura T, Sakagami M, Nakase T, Kubo T, Kitamura Y, Nomura S. Localization of osteopontin in the otoconial organs of adult rats. Hear Res 1994;79:99–104. [PubMed: 7806488]

Takumida M, Harada Y. Development of the utricular macula in the mouse. Arch Otorhinolaryngol 1984;241:9–15. [PubMed: 6151388]

Trune DR, Lim DJ. The behavior and vestibular nuclear morphology of otoconia-deficient pallid mutant mice. J Neurogenet 1983;1:53–69. [PubMed: 6681441]

Verpy E, Leibovici M, Petit C. Characterization of otoconin-95, the major protein of murine otoconia, provides insights into the formation of these inner ear biominerals. Proc Natl Acad Sci U S A 1999;96:529–534. [PubMed: 9892667]

Wang Y, Kowalski PE, Thalmann I, Ornitz DM, Mager DL, Thalmann R. Otoconin-90, the mammalian otoconial matrix protein, contains two domains of homology to secretory phospholipase A2. Proc Natl Acad Sci U S A 1998;95:15345–15350. [PubMed: 9860971]

Wang Y, Thalmann I, Thalmann R, Ornitz DM. Mapping the mouse otoconin-90 (Oc90) gene to chromosome 15. Genomics 1999;58:214–215. [PubMed: 10366455]

Zefirov AL, Abdrakhmanov MM, Mukhamedyarov MA, Grigoryev PN. The role of extracellular calcium in exo- and endocytosis of synaptic vesicles at the frog motor nerve terminals. Neuroscience. 2006

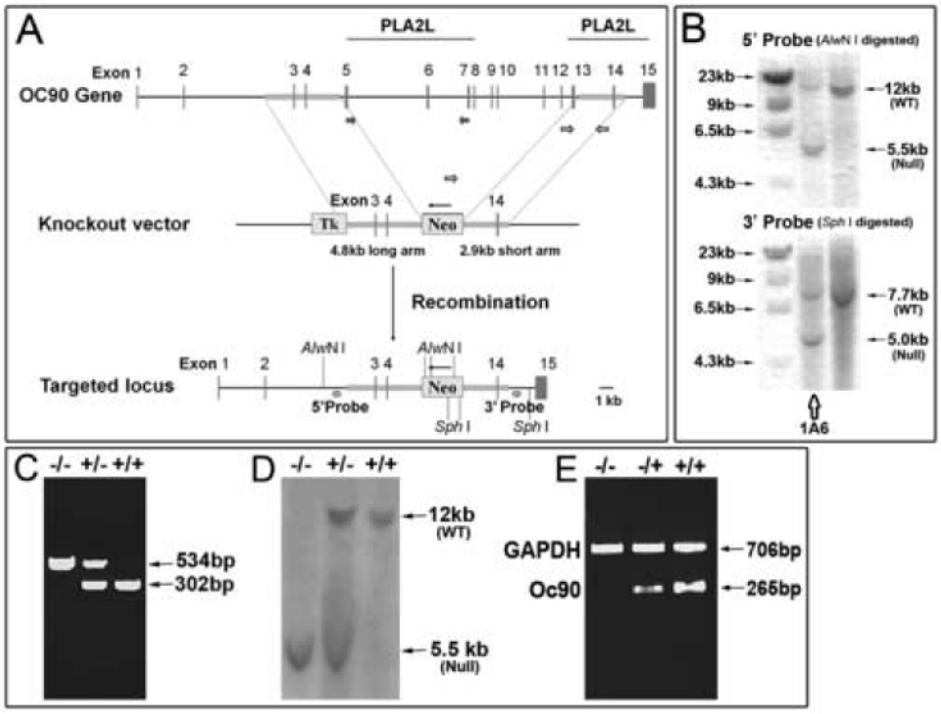

Figure 1. Targeting the Oc90 gene

(A) Design of the Oc90 targeting construct using the pPNT vector. Exons 5-13, spanning the entire first PLA_2L domain and most of the putative functional region in the 2nd PLA_2L domain, were deleted. The deletion creates an out-of-frame mutant transcript with 186bp due to a premature stop codon. Numbers indicate exons of the Oc90 gene and thin arrows directions of genes. (B) Confirmation of the initially identified positive clones by second-round Southern blotting. Clone 1A6 was used for injection of C57Bl6/J blastocysts. (C, D) Genotyping of Oc90 mutant pups by multiplex PCR (C) and Southern blotting (D) of tail DNA. PCR primers are denoted by unfilled block arrows in (A). (E) Inactivation of Oc90 transcript in Oc90 null mutants (1 month old) as confirmed by semi-quantitative multiplex RT-PCR analysis of inner ear tissues. Oc90 RT-PCR primers are located in the deleted region as denoted by filled block arrows in (A). Inactivation of Oc90 protein is shown in Figure 4E.

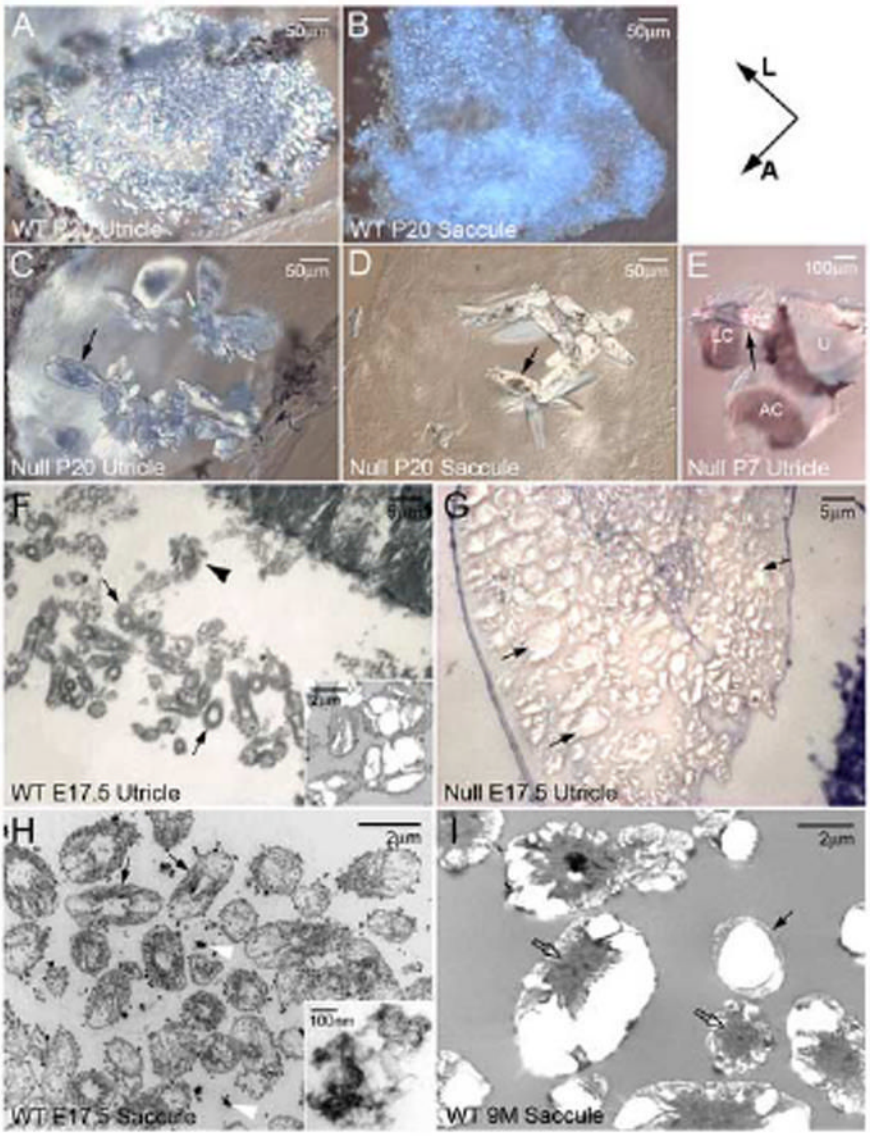

Figure 2. Formation of giant otoconia (C, D, E, G) in Oc90 null mice

The giant otoconia have prominent mineral deposits (arrows in C, D) and form aggregates (G). These crystals are loose and not securely anchored to the otoconial membrane. Some become associated with the roof of the utricle and saccule (arrow in E, utricle) and the semi-circular canals. A-E show whole-mount utricle or saccule. (F-I) Organization of the organic matrix in Oc90 wt otoconia and its absence in Oc90 null otoconia. (F, G) are semi-thin (500nm), Toluidine-stained sections of otoconia seeds viewed under a light microscope and (H, I) are ultra-thin (85 nm) sections of otoconia viewed under TEM. The size of the giant null otoconia shown in G is estimated to be over 1,000× larger than the wt ones shown in F. Thin arrows in F, H and I denote the organic matrix that embeds the immature crystallites but is absent in the null otoconia, which only have the inorganic crystallites (arrows in G). Inset in F is a TEM micrograph showing the fusion of several crystallites to become the mature otoconium, as occasionally seen in the E17.5 vestibule and abundantly seen in adults (I). The adult vestibule

has occasional otoconia seeds that are embedded in the organic matrix (thin arrow in I), which likely arise from neogenesis. The embedded wt crystallites are different than the matrix vesicles (arrowhead in F). These vesicles appear to contain organic particles that stain intensely with Toluidine Blue. Such organic particles may become incorporated into the developing otoconia seeds as shown by white arrowheads in (H) and inset in (H). Block arrows in I denote the centrally located organic matrix of the mature otoconium. A, anterior; AC, anterior canal; L, lateral; LC, lateral canal; U, utricle.

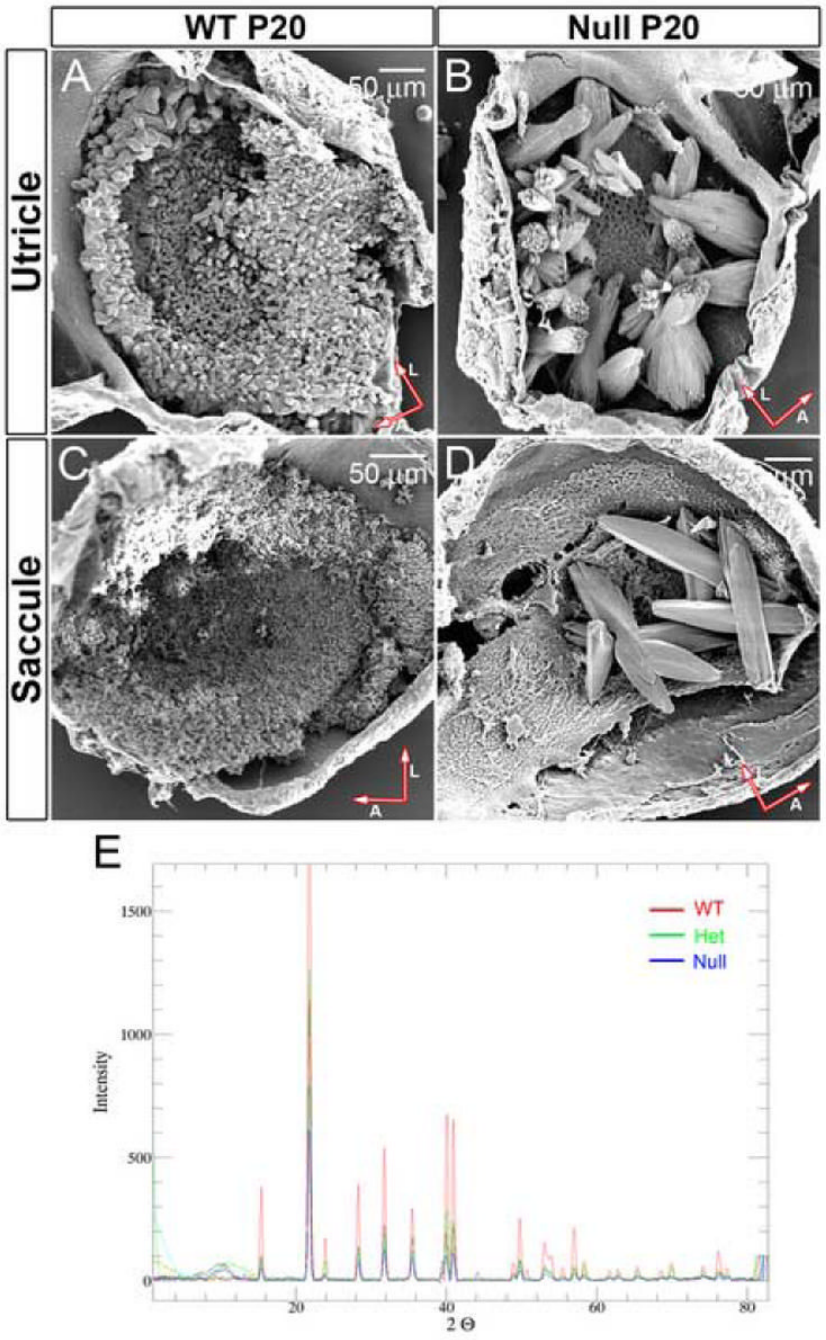

Figure 3. (A, B, C and D) Scanning electron microscopy of Oc90 null and wt otoconia

A comparison of their sizes is listed in Table 1. The mutant otoconia have surface folds similar to "rock formation" seen in nature. The distortion in otoconia morphology is worse in the utricle than the saccule. Not all null utricles and saccules have as many crystals as shown. Arrows indicate orientation of whole-mount tissues (A, anterior; L, lateral).

(E) X-ray powder diffraction analysis of Oc90 null, het and wt crystalline structures (3 months-old mice). For each sample a series of frames were taken at increments of 10 degrees 2θ while rotating φ. The frames were then merged using the PhaseID module of the Bruker-AXS control program and the resulting pattern of peaks was integrated to produce a powder diffraction pattern. Otoconia from all three genotypes show the same peak distribution pattern of the

calcitic crystalline structure. Large variations in the relative peak intensities are expected of samples with a high degree of preferred orientation such as otoconia crystallites.

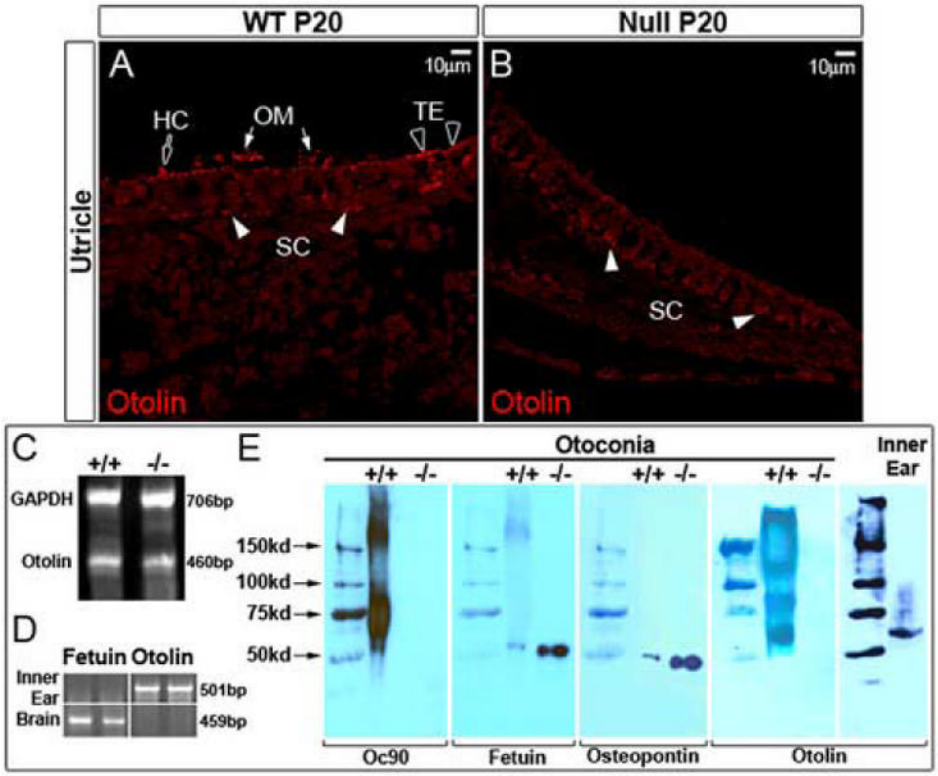

Figure 4. Examination of minor otoconins in the Oc90 wt and null vestibule

Otolin protein (60kD) is present in otoconial crystals (E) and membranes (OM) (arrows in A) and the pericellular matrix of hair cells (block arrow) and supporting cells (filled arrowheads) in the wt utricle and saccule (the utricle is shown). A few cells in the transitional epithelium (TE) have intracellular staining (unfilled arrowheads in A). However, otolin is absent (or greatly reduced to below the detection level) in the OM and giant crystals in the Oc90 null vestibule (B, E). Decalcified cross sections of the utricle and saccule were used for immunostaining with an antibody raised against the C-terminal unique peptide of murine otolin. Semi-quantitative multiplex RT-PCR detected expression of otolin mRNA in 1-month-old Oc90 wt and null inner ear epithelial tissues (C). Other minor otoconins, including fetuin-A and osteopontin, are present in the null crystals (E). Approximately 3.7μg of wt and 5.1μg of null otoconia protein was loaded. The same membrane was detected with antibodies against Oc90, fetuin-A (55 kD) and osteopontin (50 kD). Similar to collagen X, otolin forms extra-cellular multimers in otoconia crystals but exists as a monomer intra-cellularly in the inner ear epithelium. Also shown in (E) is confirmation of inactivation of Oc90 protein in null otoconia (1 month old) as examined by Western blotting using an antibody against the N-terminal peptide of the secreted protein. (D) Absence of fetuin-A (labeled as fetuin in D, E) and presence of otolin transcripts in the inner ear epithelium as determined by RT-PCR of tissues from C57 pups (P7) (assays were done in triplicates, but only duplicates are shown). The opposite is true in the brain: feuin-A transcript is present whereas otolin absent in the tissue. HC, hair cell; OM, otoconial membrane; SC, supporting cell; TE, transitional epithelium.

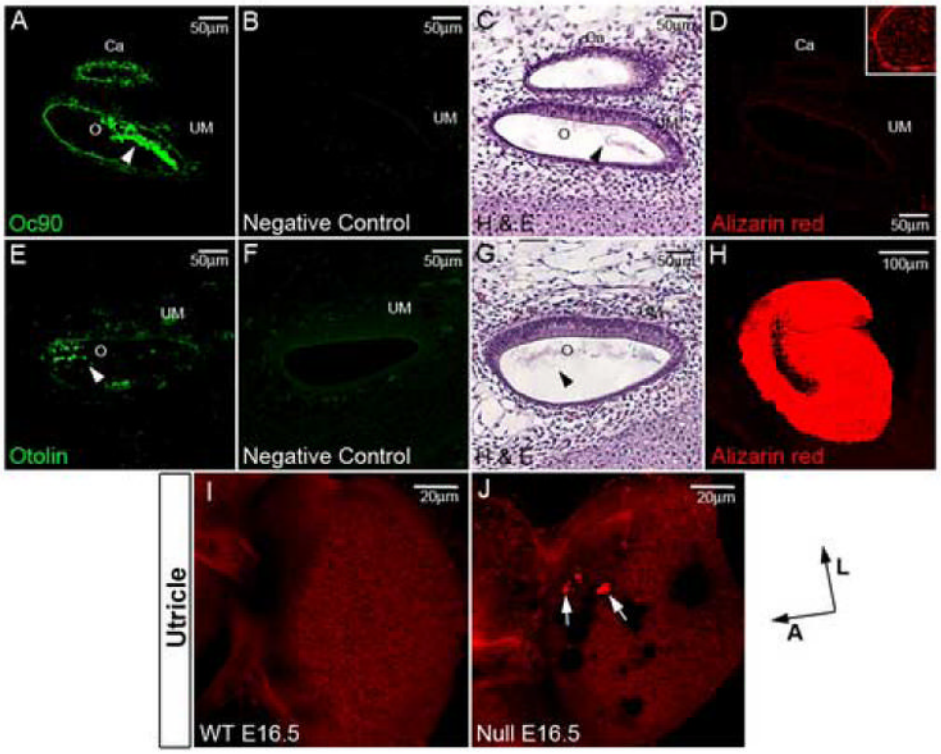

Figure 5. Otoconia seeds in the wt utricle

Formation of the organic matrix precedes the deposition of $CaCO_3$ crystallites. Otoconia seeds in the E16.5 wt utricle have a high level of Oc90 (arrowhead in A), a low level of otolin (arrowhead in E), an absence of or extremely low levels of $CaCO_3$ (D). Bones on the same sagittal section are stained (stained tibia is shown as inset in D). Oc90 is known to be expressed all over the non-macular epithelium. (A) and (D) are the same confocal view. A-D have the same magnification and are immediately adjacent sagittal sections, as do E-G. (C, G) Sections adjacent to (A) and (E), respectively, were stained with H&E. Arrowheads show otoconia seeds. (B, F) Pre-immune sera were used in the negative controls (adjacent sections) to ensure that the staining in otoconia was not due to trapped reagents (null tissues only had a few giant crystal particles that were sometimes lost during sectioning). (H) P0 whole-mount utricle stained robustly with Alizarin Red Complexone. (I, J) Whole-mount Alizarin Red Complexone staining for otoconia seeds in the E16.5 wt (I) and null utricle (J). There is no staining in the wt vestibule, but moderate to strong staining in the null tissue. The aggregated null seeds (denoted by arrows in J) increase the amount of $CaCO_3$ for positive staining. Arrows at the bottom right corner indicate orientation of whole-mount tissues (A, anterior; L, lateral). Ca, canal; O, otoconia seeds; UM, utricular macula.

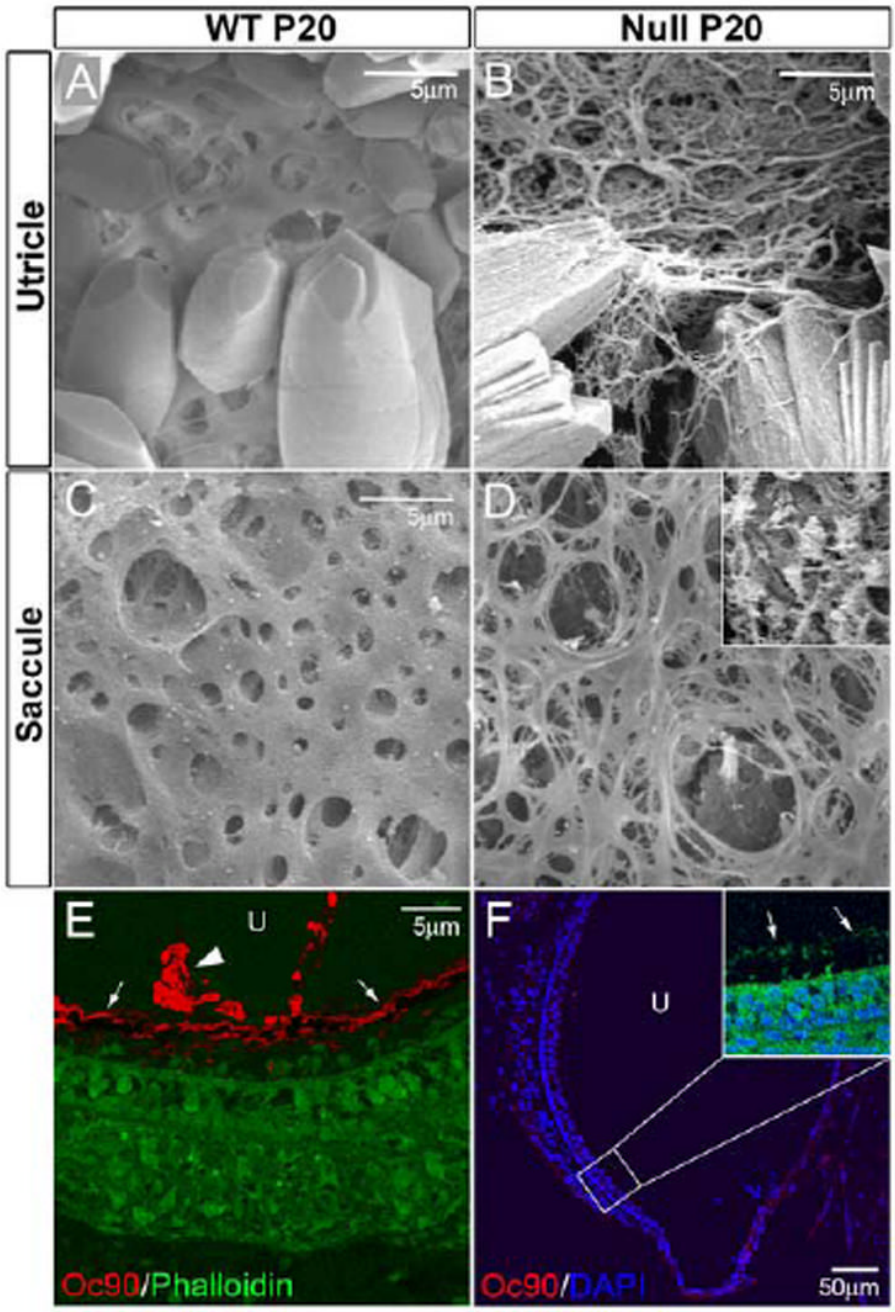

Figure 6.

(A-D) Abnormal otoconial membranes (OM) in the utricle and saccule of Oc90 null mice. The membranes have more delicate fibers in the honeycomb layer, are less compact, brittle and frequently broken. Shown in inset in D is the flora-like structure that is also seen in the *hslt* saccule (Kiss et al., 2006). (E, F) Immunostaining shows the presence of Oc90 protein in the OM (arrows in E) in the wt vestibule (utricle shown), but not in the null vestibule (null OM is stained with phalloidin as denoted by arrows in inset in F). Arrowhead in E denotes Oc90-stained otoconia. The mutant Oc90 protein (6.6 kD), assuming translated and stable, is not expected to be incorporated in the crystals or OM as it lacks any functional domains. U, utricle.

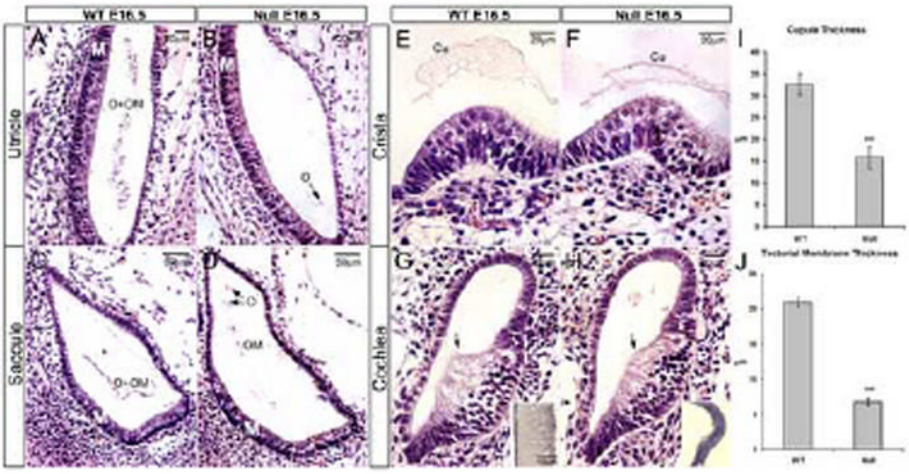

Figure 7.

Normal epithelial cellular morphology in H & E stained E16.5 inner ear sections of Oc90 wt and null mice. Compared with the normal minute seeds in the wt vestibule (A, C), the null utricle and saccule only have several large otoconia particles (denoted by arrows in B, D) and remnants of otoconial membranes (labeled OM in D) which stain much lighter for H&E. The much lighter staining is likely due to the absence of the organic matrix in the crystals and a reduction of OM. Notably, the cupula (Cu in E and F) and the tectorial membrane (insets in G & H are 9 months-old tissues) are significantly thinner in the null inner ear. The acellular matrix (arrows in G, H) adjacent to the inner hair cell in the developing cochlea that gives rise to the future tectorial membrane is also significantly thinner. The bar diagrams in I and J represent the actual thickness of the membranes (n=6). ***, $p<0.0001$. Cu, cupula; O, otoconia; OM, otoconial membrane; M, macula (including hair/supporting cells).

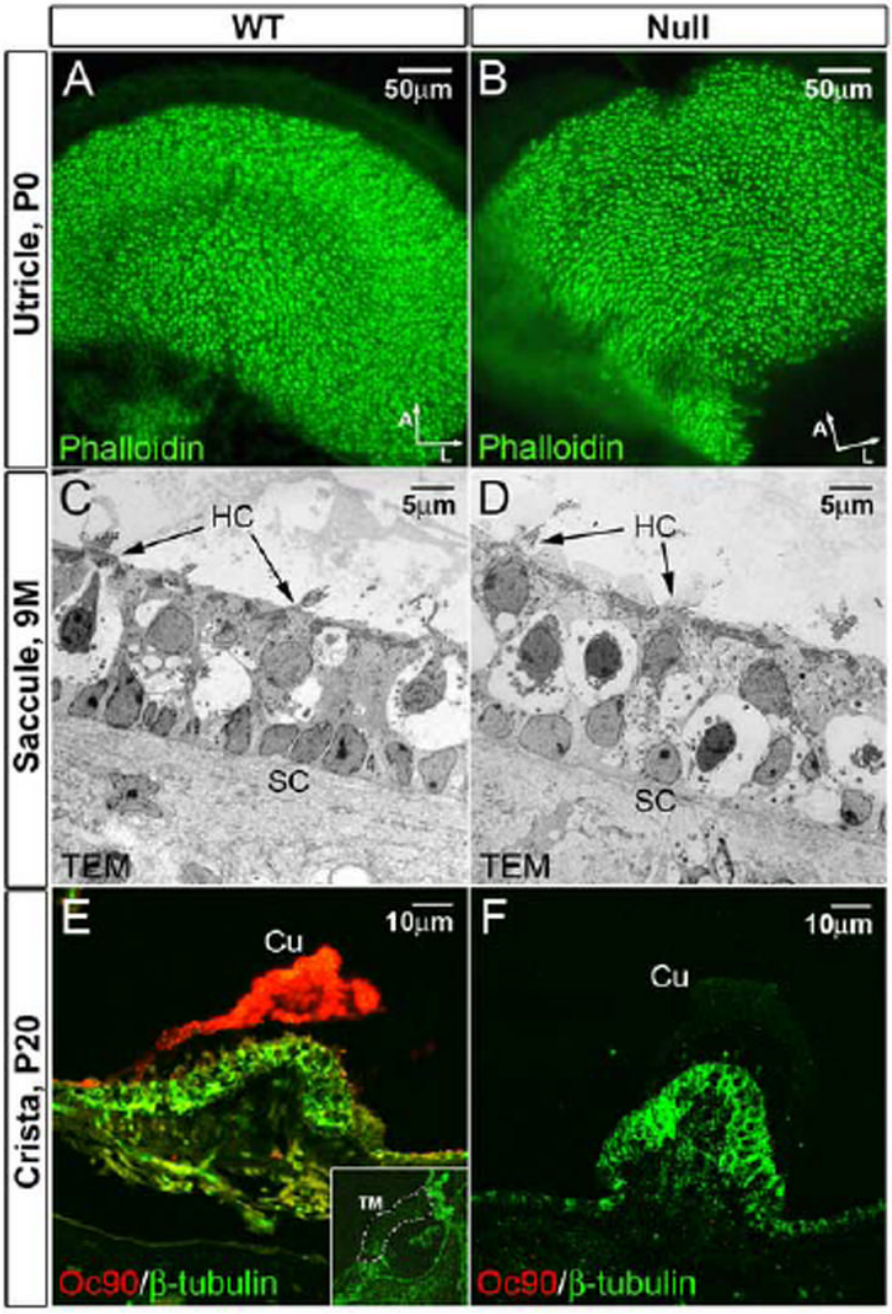

Figure 8.

(A, B) Normal density, organization and appearance of stereocilia in the Oc90 null vestibule as demonstrated by phalloidin-stained whole-mount utricle (P0). Arrows indicate orientation of whole-mount tissues (A, anterior; L, lateral). (C, D) Normal ultrastructure of the macular epithelial cells in Oc90 null mice (9 months old) as demonstrated by transmission electron microscopy. The amorphous gel-like structure above the macular sensory epithelium is also normal in the Oc90 null vestibule (only lightly visible in D due to the lighter background). (E, F) Oc90 is abundantly present in the wt cupula (P20 shown) but not in the null tissue. Shown in inset in (E) is the absence of Oc90 in the P20 wt tectorial membrane (delineated by dotted

lines). The E16.5 wt tectorial membrane also has negative Oc90 signals. Cu, cupula; HC, hair cells; SC, supporting cells; TM, tectorial membrane.

Table 1

Otoconia sizes in the Oc90 wt & null vestibule (1 month-old mice sampled, n=25)

		Length (μm)	Width (μm)
Utricle	WT-peripheral	24.5±5.2	13.0±3.2
	WT-central	16.2±3.0	6.8±1.5
	Null	155.6±56.7*	68.8±35.7*
Saccule	Wt	4.0±0.7	1.9±0.3
	Null	146.9±58.9*	35.6±5.3*

* $p<0.001$

Table 2

Identified and validated murine otoconins and accession numbers

	Otoconin	# of identified peptides	Accession #
Utricle	Oc90/Oc95	31	45545407/4092677
	Fetuin-A	2	2546995
	Otolin	4	51708061
Saccule	Oc90/Oc95	25	45545407/4092677
	Fetuin-A	2	2546995
	Otolin	2	51708161

Note: Oc90 has been previously identified and characterized (Verpy et al., 1999;Wang et al., 1998).